Progress In Electromagnetics Research B, Vol. 59, 205–217, 2014

Experimental Characterization of the Propagation Channel along a Very Large Virtual Array in a Reverberation Chamber

Andrés Alayón Glazunov[1, *], Sathyaveer Prasad[2], and Peter Händel[3]

Abstract—We show that the combined use of radio frequency absorbers and directive antennas can produce significant changes of the radio propagation channel properties along the positions of a virtual array inside a reverberation chamber. A multidimensional characterization of the channel was performed at 40 antenna positions with spacing of 0.233λ at 1 GHz. The average power, the Ricean K-factor, the coherence bandwidth, the r.m.s. delay spread, the mean delay, the beamforming power angle spectrum and array antenna correlation have been studied for different arrangements in the reverberation chamber. The analysis shows that the joint average over time and frequency channel behavior is, as expected, rather homogeneous along the very large array. However, individual realizations of the channel present a pronounced selective behavior in space, time and frequency with parameters varying along the positions of the virtual array suggesting that a heterogeneous behavior of the radio channels can be emulated in reverberation chambers. An important application of the presented study comprises testing of antenna array designs and algorithms in multipath environments. Further development may lead to Over The Air testing of Multiple Input Multiple Output antenna systems of various sizes, i.e., from small to very large arrays.

1. INTRODUCTION

Multiple Input Multiple Output (MIMO) antenna systems provide improved data throughput to users by increasing the number of antennas at the base station and at the user device. The standardized implementation of this technology has been available for a time now [1]. Recently, it has been proposed to extend the number of antennas on the base station side to "massive" proportions in multi-user scenarios known as Very Large Multiple Input Multiple Output (VLM) systems [2, 3]. In VLM, a large number of antennas (e.g., 40–400) are employed at the base stations for serving simultaneously several user devices. One of the main advantages of this technique is that it is not necessary to have multi-antenna user devices, thus potentially reducing cost and complexity.

The behavior of the VLM radio propagation channel has been scarcely investigated as opposed to conventional MIMO channels. The propagation channel measurements can be performed by means of virtual Uniform Linear Array (ULA) simulating the VLM base station. Virtual arrays assume that no coupling exists between the antenna elements. In practice there is always coupling; however, this idealization can serve as a first order approximation of practical array antennas. This assumption can be practically sound for the large spatial separation on VLM antennas, e.g., 0.233λ. Indeed, though coupling may not be negligible, it has a major impact on MIMO capacity only when the separation distance is less than 0.2λ as shown in [4]. In [5, 6], the channel characteristics were studied in terms of the average receive power, the Ricean K-factor, the singular value distribution, the antenna correlation, the angular power spectrum and the near field effects. These first studies suggest, as expected, that the

Received 12 March 2014, Accepted 8 April 2014, Scheduled 18 April 2014

* Corresponding author: Andrés Alayón Glazunov (aag@ee.kth.se).

[1] Division of Electromagnetic Engineering, Royal Institute of Technology (KTH), Teknikringen 33, Stockholm 100 44, Sweden. [2] Gävle University College and Signal Processing Lab, KTH Royal Institute of Technology, Stockholm, Sweden. [3] ACCESS Linnaeus Centre, Signal Processing Lab, KTH Royal Institute of Technology, Stockholm, Sweden.

channel characteristics vary along the very large ULA. However, more experimental data is needed to really understand the properties of these channels.

In addition, though field measurements give a real time estimate of the performance of a device in a real propagation channel they are not repeatable. Thus, they cannot be used as a standard reference method for measuring the radiated performance of a wireless device, whether it is a mobile terminal or a base station. Here, Over The Air (OTA) testing techniques become an indispensable tool for performance evaluation of MIMO antenna systems. The main purposes with OTA testing is to evaluate the performance of MIMO devices under laboratory conditions that emulate realistic propagation channel characteristics. OTA testing techniques are often divided into two main groups depending on the type of measurement chamber used [7]. On one hand, we have the *anechoic* chamber techniques where the walls of the chambers absorb the radiated energy allowing to generate a propagation channel with the desired distribution of directional channel parameters, e.g., the Angle of Arrival (AoA). While, on the other hand we have the *reverberation* chamber (RC) techniques where the walls are highly reflective (metallic) and the resulting field is more isotropically distributed. In this paper, we focus our attention on the latter technique and we look at ways to use relatively large RCs to emulate various channels.

The standardized type of channel often recreated in RC is known as the rich scattering isotropic environment [8]. This environment presents an isotropic AoA distribution, a Rayleigh distributed field magnitude and an exponential decay of the power delay profile (see [9, 10] and references therein). However, the first available studies performed with a virtual ULA has suggested that the rich isotropic channel may not be, as expected, a typical VLM channel [5, 6]. A few studies, like the ones presented in [11, 12] investigate ways to generate Rice and nonisotropic channels in relatively small-size RC. However, the propagation channel inside relatively large reverberation chambers has not been investigated previously for evaluating array antennas of any size. There is a lack of knowledge pertaining the simulation of VLM channels in such environments. Hence, there is a need to fill this gap of knowledge.

Our main goal is to show that by means of a combined use of radio frequency absorbers and directive antennas, different characteristics of the propagation channel can be emulated along a very large virtual ULA. We provide an experimental multi-dimensional characterization of the propagation channel in a relatively large reverberation chamber. We illustrate our results on the basis of the analysis of what we call global statistics and local statistics. The standardization of VLM OTA tests and the standardized use of relatively large RC to emulate various channel conditions for OTA testing might well be in a relatively distant future. However, it is highly relevant to study the propagation environment in relatively large RCs and the means of adapting them to our needs at an early stage. Moreover, findings of this paper can be used to assess the performance of antenna designs and algorithms in the broad sense too, i.e., not only for VLM.

2. RADIO PROPAGATION CHANNEL PARAMETERS

The variation of the wave field inside a reverberation chamber can be modeled as a multidimensional stochastic process in the frequency, in the space and in the time domains [13, 14]. It is this spatio-temporal frequency response that interests us in order to evaluate the properties of the VLM channel inside the chamber [15]. We present next some well-known functions used for this characterization for the sake of completeness.

Let's assume now that the transmit antenna is at a fixed position, but the receive antenna is moved along a line at discrete positions inside the chamber emulating a very large virtual ULA. Hence, we can denote the position-dependent and time-variant radio propagation channel (includes the antennas and the propagation channel) transfer function as follows

$$H(f, x, t) = S_{21}. \tag{1}$$

where the S_{21}-parameter, i.e., the transmission scattering parameter, is the measured quantity, f the frequency, x the different positions inside the chamber (in our case they correspond to different positions along a very large virtual ULA), and t the time. The corresponding channel impulse response is often used to characterize the radio propagation channel, but also to quantify the losses in the reverberation chamber [10] and is obtained as $h(\tau, x, t) = \mathsf{F}_f^{-1}\{H(f, x, t)\}$, where $\mathsf{F}_f^{-1}\{\}$ denotes the inverse Fourier

transform operator. Furthermore, as far as we are concerned with the statistics of (1), we can assume the well-established two-term model for the variation of the channel

$$H(f,x,t) = H_d(f,x,t) + H_s(f,x,t), \tag{2}$$

where $H_d \doteq S_{21,d}$ and $H_s \doteq S_{21,s}$ are the deterministic and stochastic components, respectively. We use $\doteq$ to denote a defining relationship. The deterministic term models the unstirred component of the coupling between the transmit and receive antennas, i.e., the dominating LOS (line-of-sight) component or a strong reflection. The stochastic term characterizes the NLOS (none-LOS) component, i.e., the stirred wave components resulting from the continuous movement of the stirrers. Hence, the corresponding impulse response can be represented as

$$h(\tau,x,t) = h_d(\tau,x,t) + h_s(\tau,x,t). \tag{3}$$

A well-established approach to studying the properties of a propagation channel is to extract a set of condensed parameters from $H(f,x,t)$ and $h(\tau,x,t)$ as we proceed next [17].

2.1. Mean Power and *K*-Factor

The field distributions inside a reverberation chamber can be modeled by the complex Gaussian probability distribution functions [16]. Therefore, to characterize the field magnitude distribution statistics of various multipath components arriving at the receive antenna we use the Rice probability distribution function (pdf) [13, 14, 18]. The Ricean pdf is characterized by two parameters: the average power which is given by $P = \mathsf{E}\{|S_{21}|^2\}$ and the Ricean K-factor defined as the power ratio of the fixed and fluctuating components, i.e., the power of the dominant path P_d and the power of all other paths P_s, i.e., $K = P_d/P_s$, where $P_d = |S_{21,\mathrm{d}}|^2$, $P_s = \mathsf{E}_t\{|S_{21,\mathrm{s}}|^2\}$, $P = P_d + P_s$ and $\mathsf{E}_t\{.\}$ denotes mathematical expectation or average operator acting across the time dimension t. In all the calculations, $\mathsf{E}_q\{\alpha(q)\}$ is replaced by the arithmetic mean, i.e., the sample mean based on the samples of variable α at instances q, where q can be time, position, frequency or time delay.

We use in our analysis the following definitions of the average power P and the corresponding definitions of K-factors along the different signal dimensions, i.e., frequency, delay and position

$$P(f) = \mathsf{E}_x\left\{\mathsf{E}_t\left\{|H(f,x,t)|^2\right\}\right\}, \tag{4a}$$

$$P(\tau) = \mathsf{E}_x\left\{\mathsf{E}_t\left\{|h(\tau,x,t)|^2\right\}\right\}, \tag{4b}$$

$$P(x) = \mathsf{E}_\tau\left\{\mathsf{E}_t\left\{|h(\tau,x,t)|^2\right\}\right\}, \tag{4c}$$

$$K(f) = \mathsf{E}_x\left\{\mathsf{K}_{\boldsymbol{t}}\left\{H(f,x,t)\right\}\right\}, \tag{5a}$$

$$K(\tau) = \mathsf{E}_x\left\{\mathsf{K}_{\boldsymbol{t}}\left\{h(\tau,x,t)\right\}\right\}, \tag{5b}$$

$$K(x) = \mathsf{E}_\tau\left\{\mathsf{K}_{\boldsymbol{t}}\left\{h(\tau,x,t)\right\}\right\}, \tag{5c}$$

where the pairs $(P(f),K(f))$, $(P(\tau),K(\tau))$ and $(P(x),K(x))$ denote *global statistics* of Rician distribution parameters studied as a function of frequency, delay and positions along the virtual linear array (or in general a position within the chamber), respectively. $\mathsf{K}_{\boldsymbol{t}}\{H(t)\}$ shall be understood as an operator acting on the function $H(t)$ along dimension t and giving a K-factor estimate for which we use [20].

In addition to the expected value of the average power and the K-factor, we compute their Coefficient of Variation denoted by CV with a subscript for the corresponding quantity. The Coefficient of Variation is defined as the ratio of the standard deviation to the expected value of a random variable. The obtained measure of dispersion is in this way independent from the variable's measurement unit. The higher the Coefficient of Variation, the greater the dispersion in the studied variable. This is an important parameter to evaluate the impact of different arrangements on the channel behavior.

$$CV_P(f) = \frac{\sqrt{\mathsf{Var}_x\{\mathsf{E}_t\{|H(f,x,t)|^2\}\}}}{\mathsf{E}_x\{\mathsf{E}_t\{|H(f,x,t)|^2\}\}}, \tag{6a}$$

$$CV_P(\tau) = \frac{\sqrt{\mathsf{Var}_x\{\mathsf{E}_t\{|h(\tau,x,t)|^2\}\}}}{\mathsf{E}_x\{\mathsf{E}_t\{|h(\tau,x,t)|^2\}\}}, \tag{6b}$$

$$CV_P(x) = \frac{\sqrt{\mathsf{Var}_\tau\{\mathsf{E}_t\{|h(\tau,x,t)|^2\}\}}}{\mathsf{E}_\tau\{\mathsf{E}_t\{|h(\tau,x,t)|^2\}\}}, \tag{6c}$$

$$CV_K(f) = \frac{\sqrt{\mathsf{Var}_x\{\mathsf{K}_t\{H(f,x,t)\}\}}}{\mathsf{E}_x\{\mathsf{K}_t\{H(f,x,t)\}\}}, \tag{7a}$$

$$CV_K(\tau) = \frac{\sqrt{\mathsf{Var}_x\{\mathsf{K}_t\{h(\tau,x,t)\}\}}}{\mathsf{E}_x\{\mathsf{K}_t\{h(\tau,x,t)\}\}}, \tag{7b}$$

$$CV_K(x) = \frac{\sqrt{\mathsf{Var}_\tau\{\mathsf{K}_t\{h(\tau,x,t)\}\}}}{\mathsf{E}_\tau\{\mathsf{K}_t\{h(\tau,x,t)\}\}}. \tag{7c}$$

It is worthwhile mentioning that in the rich scattering isotropic environment obtained in a reverberation chamber with perfect mode stirring $P(\tau, x)$ is given by an exponentially decaying function as a function of the delay τ at any position x within the chamber [10]. This parameter is especially important in the analysis and design of OFDMA MIMO that produces orthogonal flat fading subchannels in the frequency domain.

2.2. Coherence Bandwidth, Delay Spread and Mean Delay

Another fundamental parameter of the radio propagation channel is the coherence bandwidth [10]. Now, we assume that the channels measured in RC are WSSUS (Wide Sense Stationary Uncorrelated Scattering) stochastic process, i.e., WSS means that the first two moments of the distribution (i.e., mean and variance) are independent of time and US means that the path gains corresponding to different delays are uncorrelated. We can compute the instantaneous position-dependent frequency correlation function defined as $\tilde{\mathcal{R}}_H(\Delta f, x, t) = \mathsf{F}_\tau\{|h(\tau,x,t)|^2\}$, where $\mathsf{F}_\tau\{\}$ denotes the direct Fourier transform operator. Hence, the instantaneous position-dependent coherence bandwidth $B_k(x,t)$ is obtained at a user defined level k as the smallest Δf satisfying $|\tilde{\mathcal{R}}_H(\Delta f, x, t)| < k|\tilde{\mathcal{R}}_H(0,x,t)|$.

Information about local (small-scale) channel dispersion can be obtained from

$$\sigma_\tau(x,t) = \sqrt{\frac{\int_0^\infty \tau^2 |h(\tau,x,t)|^2 \, d\tau}{\int_0^\infty |h(\tau,x,t)|^2 \, d\tau} - \mu_\tau^2(x,t)}, \tag{8}$$

$$\mu_\tau(x,t) = \frac{\int_0^\infty \tau |h(\tau,x,t)|^2 \, d\tau}{\int_0^\infty |h(\tau,x,t)|^2 \, d\tau}, \tag{9}$$

where $\sigma_\tau(x,t)$ and $\mu_\tau(x,t)$ are the instantaneous position-dependent r.m.s. (root mean squared) delay spread and the instantaneous position-dependent mean delay, respectively. In a similar way as above we also define global statistics for the coherence bandwidth, r.m.s. delay spread and mean delay. The integrals in (8) and (9) are replaced by sums in the discrete case. The expected values $B_k(x)$, $\sigma_\tau(x)$ and $\mu_\tau(x)$ are computed as follows

$$B_{0.5}(x) = \mathsf{E}_t\{B_{0.5}(x,t)\}, \tag{10}$$

$$\sigma_\tau(x) = \mathsf{E}_t\{\sigma_\tau(x,t)\}, \tag{11}$$

$$\mu_\tau(x) = \mathsf{E}_t\{\mu_\tau(x,t)\}, \tag{12}$$

and the corresponding Coefficient of Variations are given by

$$CV_{B_{0.5}}(x) = \frac{\sqrt{\mathsf{Var}_t\{B_{0.5}(x,t)\}}}{\mathsf{E}_t\{B_{0.5}(x,t)\}}, \tag{13}$$

$$CV_{\sigma_\tau}(x) = \frac{\sqrt{\mathsf{Var}_t\{\sigma_\tau(x,t)\}}}{\mathsf{E}_t\{\sigma_\tau(x,t)\}}, \tag{14}$$

$$CV_{\mu_\tau}(x) = \frac{\sqrt{\mathsf{Var}_t\{\mu_\tau(x,t)\}}}{\mathsf{E}_t\{\mu_\tau(x,t)\}} \tag{15}$$

All of the above parameters depend on the position along the very large virtual ULA. These parameters will be used to characterize the variability of the coherence bandwidth and delay spread at the different positions inside a reverberation chamber.

2.3. Antenna Correlation

The analysis of MIMO antenna systems depends on the correlation between the signals received by different antenna elements. In our specific case, the correlation will depend only upon the field distribution in the chamber, but not on the antenna coupling since we consider a virtual linear array. Even, though the process along the array can not be regarded as WSS in general we can still analyze product-moment correlation coefficient or rather its average. The frequency-dependent correlation coefficient between the signals received at positions x_i and x_j is defined as

$$\rho_{ij}(f) = \frac{\mathsf{E}_t\{(H(f,x_i,t)-\mu_i(f))(H(f,x_j,t)-\mu_j(f))^*\}}{\sigma_i(f)\sigma_j(f)}, \tag{16}$$

where $i,j = 1,2,\ldots,40$ are indices indicating the antenna position within the array and $\mu_{i(j)} = \mathsf{E}_t\{(H(f,x_{i(j)},t)\}$, and $\sigma^2_{i(j)} = \mathsf{E}_t\{(H(f,x_{i(j)},t)-\mu_{i(j)}(f))^2\}$ denote the mean and variance, respectively. Hence, we can compute the average of the absolute value of the correlation coefficient $\rho_{ij} = \mathsf{E}_f\{|\rho_{ij}(f)|\}$, where the average is taken over the measurement bandwidth. For a correlation coefficient we have that $0 \leq \rho_{ij} < 1$ if $i \neq j$ and $\rho_{ii} = 1$.

2.4. Average Power, K-Factor and Beamforming AoA Spectrum

In addition to the above defined global statistics we also evaluate functions that present the behavior of the channel along the virtual array at the single frequency $f = f_0$. This is done to investigate the channel behavior along the virtual array for an individual or local channel realization in contrast to the averaged behavior. We define the instantaneous position-dependent power at a single frequency (narrowband) as $P(f_0,x,t) = |H(f_0,x,t)|^2$, the position dependent K-factor is defined as $K(f_0,x) = \mathsf{K}_{\boldsymbol{t}}\{H(f_0,x,t)\}$. The Power Angle Spectrum (PAS) is computed based on the Bartlett beamforming AoA Spectrum [21].

3. MEASUREMENT SETUP

The schematic representation of the measurement setup is shown in Fig. 1. The reverberation chamber used in the measurement campaign is a customized EOLE Siepel chamber available in-house at the Electromagnetic Engineering Department, KTH Royal Institute of Technology, Stockholm. An inside

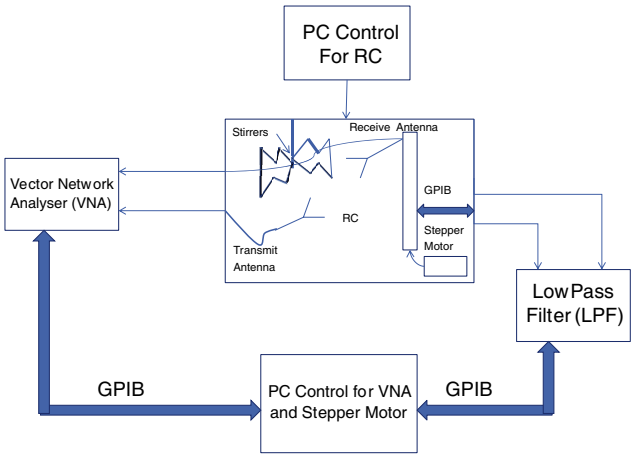

Figure 1. Block-diagram showing measurement setup for propagation measurements in RC.

Figure 2. Inside view of RC: showing LPA, bowtie antenna on horizontal slider and stirrers.

view of the chamber is shown in Fig. 2. The internal dimensions of the reverberation chamber are approximately $4.34 \times 3.69 \times 4.06\,\mathrm{m}^3$. Two Personal Computers (PCs) were used during the measurements as shown in Fig. 1. PC1 was used to control the stirring paddles, which were rotated at the angular speed $\omega_{\mathrm{stir}} = 35°/\mathrm{s}$. PC2 was used to control a Vector Network Analyzer (VNA) and a stepper motor driving a load on a horizontal slider placed inside the reverberation chamber.

The measurements were performed at 1 GHz with a Log Periodic Array (LPA) as transmit antenna and a bowtie antenna as receive antenna. A very large virtual ULA was emulated by mounting the bowtie antenna on the horizontally moving slider. The slider was moved stepwise to 40 positions separated 0.233λ apart, i.e., 6.99 cm at 1 GHz, covering a total array length of 9.087λ or 2.73 m. In order to produce channels with different K-factors, according to [14], the LPA antenna was kept at a fixed position, but measurements were performed at two different orientations. First, the LPA was directed towards a point at the slider (i.e., towards the bowtie antenna as shown in Fig. 2, secondly, it was directed towards the wall and away from the bowtie antenna, which hereafter we refer to as Direct and Indirect (measurements), respectively. Furthermore, in order to emulate different r.m.s. delay spread values as devised in [14], measurements were performed in an empty chamber and the chamber loaded with six 6×6 pyramidal absorbers piled one on top of each other, which we denote NA and A, respectively. Thus, we can further categorize our measurements as follows: a Line Of Sight (LOS) channel for the Direct measurements without absorbers, but three different Non Line Of Sight (NLOS) channels for the combinations Direct measurements with absorbers, and Indirect measurements with and without absorbers.

At each position along the virtual array, the coupling between the antennas, i.e., the calibrated S_{21}-parameter was measured at 401 frequency points over a bandwidth of 120 MHz giving a delay resolution of 8.33 ns and a maximum delay of 3.34 µs. While remaining at the same position on the slider this measurement was repeated 100 times under continuous rotation of the stirring paddles. Moreover, before moving to the next position the stirring paddles were returned to their initial position. In this way, we tried to emulate simultaneous measurements along the very large virtual ULA. Clearly, each time instance t corresponds to a new position of the stirring paddles. Thus, at each transmit-receive antenna configuration, i.e., fixed LPA orientation and fixed bowtie antenna position a total of 401×100 samples (frequency samples $\times$ time samples) could be measured. The total number of samples is $2 \times 2 \times 40 \times 401 \times 100$ (presence of absorber $\times$ LPA antenna orientation $\times$ bowtie antenna position $\times$ frequency samples $\times$ time samples) allowing a multidimensional analysis of the chamber response.

4. MEASUREMENT RESULTS AND ANALYSIS

In this section, we present a characterization of measured radio propagation channel properties in a reverberation chamber with focus on MIMO antenna systems including VLM systems too. The analysis is based on global and local statistics extracted according to Section 2.

The average power transfer function $P(f)$, the average power delay profile $P(\tau)$, and the average power along the very large virtual ULA base station $P(x)$ are shown in dB-scale in Figs. 3(a), (b) and (c), respectively. The corresponding coefficients of variation are shown dB-scale in Figs. 4(a), (b) and (c), respectively. As expected, the introduction of the absorbers implies a reduction of the total receive

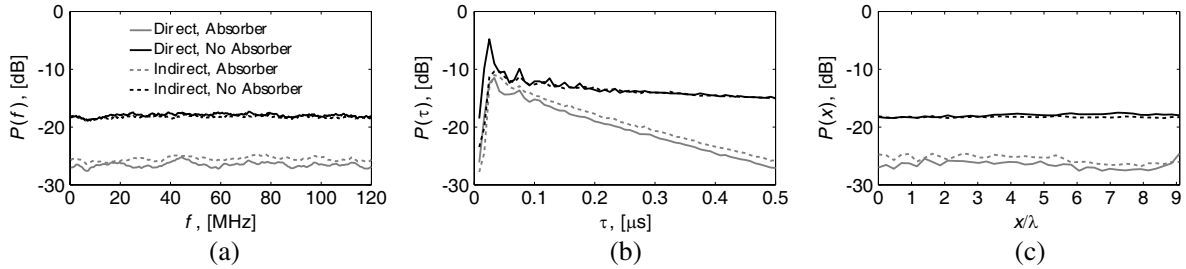

Figure 3. Expected value of the average power as a function (a) frequency, (b) time delay and (c) position along the virtual linear array. See 4(a)–4(c) for a definition.

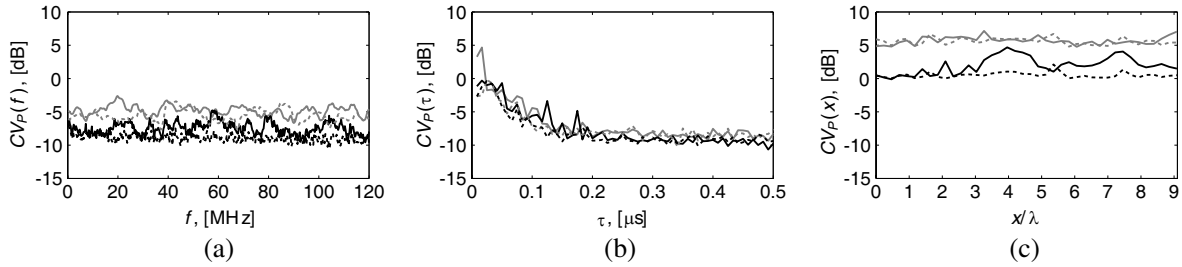

Figure 4. Coefficient of variation of the average power as a function (a) frequency, (b) time delay and (c) position along the virtual linear array. See 5(a)–5(c) for a definition.

power, in our case, it is 7.2–8.5 dB in average. Moreover, for the measurements with absorbers, the power corresponding to Direct measurements is 1 dB lower in average than the power corresponding to Indirect measurements. This is explained by the fact that the direct or LOS path of the directive LPA is absent and less power reaches the walls of the chamber and is not reflected back. It is worthwhile to note that this effect would have been less significant if an antenna with omnidirectional radiation pattern was used instead of the LPA. The average power transfer function $P(f)$ is fairly constant over the bandwidth, which is a result of the joint time and spatial averaging, i.e., averaging over different stirring paddle positions and different positions inside the chamber, respectively. The power delay profile $P(\tau)$ is not only affected by a power level reduction but also the shape is affected since the chamber decay time decreases in the presence of absorbers increasing the loading of the chamber [10]. The average power variation along the very large virtual ULA is also small; however, when the absorbers are present a larger variation is observed as compared to the case when they are absent. A decrease of power by 1 dB is observed when the position of the bowtie antenna is just behind the absorbers ($x/\lambda = 6 - 8$ in Fig. 3(c)). Hence, in principle, this variation can be made larger by proper arrangement of absorbers.

As shown in Fig. 4(a) the variability of the average power as a function of frequency is rather small for all the four considered scenarios with a low dispersion (negative dB values, i.e., $CV_P(f) < 1$) for all frequencies. The smallest variation is observed for the scenario with no absorber and LPA oriented towards the wall. This scenario would be the closest scenario to the typical rich isotropic scattering channel generated in reverberation chambers with well-stirred modes. This scenario, as we are going to see, shows consistently the most stable parameters as compared to the other three scenarios. The variability of the average power decays as a function of delay but much slower than the exponential decay of the average power as shown in Fig. 4(b). For reflections arriving at short delays, let's say $\tau \leq 0.2\,\mu$s the variability is larger than for later delays and reaches a low-level plateau. For a few short delays the variability of the average power becomes positive in dB-scale for the scenario with absorbers and LPA directed towards the virtual array. In this case the transmitted signals seem to undergo more scattering and reflections due to the presence of absorbers depending on the bowtie antenna positions. Fig. 4(c) shows that the variability of the average power as a function of position along the array is considerably larger as compared to the variability of the average power as a function of frequency or delay. However, here also the scenario with no absorber and LPA oriented towards the wall shows the least variability which not depends on the position along the array. The largest variability, though rather homogenous along the array positions, is observed for both scenarios with absorbers. Hence, we can conclude that the introduction of absorbers decrease the decay time of the impulse response increasing the variability of the average power along the virtual array positions. We also see that the variability of the power is rather heterogenous in the scenario with no absorbers and LPA pointing towards the virtual array as compared with the other three scenarios.

Figure 5 shows the average K-factor in dB-scale as a function of frequency, delay and position. As we can see from Fig. 5(a), the variation of $K(f)$ across the bandwidth is relatively small; it stays below 0 dB (i.e., $K < 1$) for all the considered scenarios. Hence, in average, the fading of different frequency components is fairly close to Rayleigh (i.e., $K = 0$). On the opposite, as shown in Fig. 5(b), the resolved paths fade rather differently. Here, we see that $K(\tau)$ peaks for paths coming with short delays (not at the shortest delay though) and thereafter decreases with oscillations as the delay increase. We can

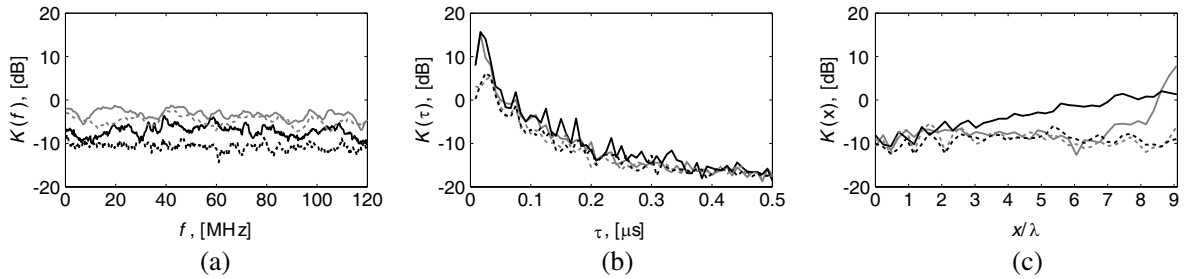

Figure 5. Expected value of the Ricean K-factor as a function (a) frequency, (b) time delay and (c) position along the virtual linear array. See 6(a)–6(c) for a definition.

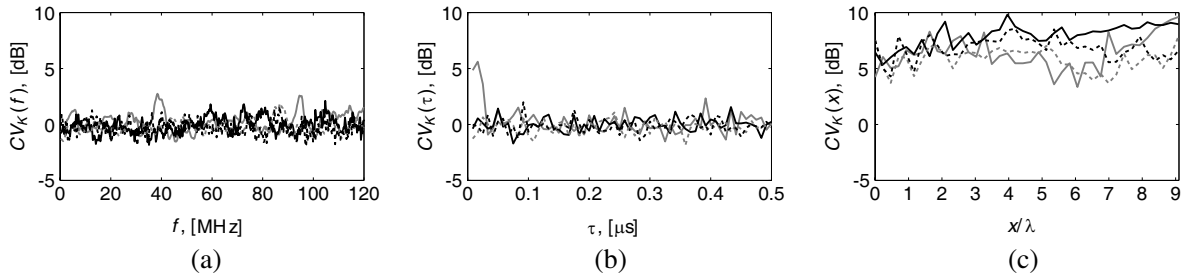

Figure 6. Coefficient of variation of the Ricean K-factor as a function (a) frequency, (b) time delay and (c) position along the virtual linear array. See 7(a)–7(c) for a definition.

roughly say that $K > 0\,\text{dB}$ is observed within the first $0.8\,\mu\text{s}$. This can be understood by realizing that the likelihood of observing unstirred components or paths incoming with short delays must be larger than for later paths. Indeed, at later delays, the waves incoming at the receive antennas are due to multiple reflections and are of fairly the same amplitudes but random phases, resulting in a more Rayleigh like fading. The largest K-factors are observed for Direct measurements independently of the presence of absorbers, which is 10 dB higher than the peak corresponding to the Indirect measurements. Fig. 5(c) reveals that the average K-factor can be made vary along the very large virtual ULA in Direct measurements; especially, when no absorber is present the average K-factor increases as the distance between the LPA and the bowtie antenna decreases [14]. For Indirect measurements, the average K-factor with and without absorbers are of the same order of magnitude (i.e., below 0 dB) and fairly constant over the whole array range.

Figure 6 shows the variability of the K-factor in dB-scale corresponding to Fig. 5. As can be seen from Fig. 6(a) the K-factor variability is larger as compared to the average power variability as function of frequency. A similar behavior is observed for the K-factor variability as compared to the average power variability as function of delay. Moreover, the K-factor variability is rather homogeneous by comparing different frequencies. On the other hand, the behavior of the K-factor variability as a function of delay does not present the decay shape observed for the average power variability as a function of delay. However, also here the variability the K-factor is much larger for a few shorter delays for the scenario with absorbers and LPA directed towards the virtual array (compare Figs. 4(b) and Figs. 6(b)). The largest K-factor variability is a function of position as shown in Fig. 6(c). As can be seen from this figure, the variability changes in a complex way along the different positions. The largest K-factor variability is observed for the scenario with no absorbers and LPA antenna directed towards the virtual array which also shows the largest dynamic range of the average K-factor as a function of delay.

Figure 7(a) shows the coherence bandwidth obtained at level $k = 0.5$ of the autocorrelation function (defined in Section 2) as a function of the position along the very large virtual ULA. As can be seen, introducing absorbers increases the coherence bandwidth which is approximately 6 times higher than without absorbers. Moreover, the use of absorbers results in a greater variation of the emulated

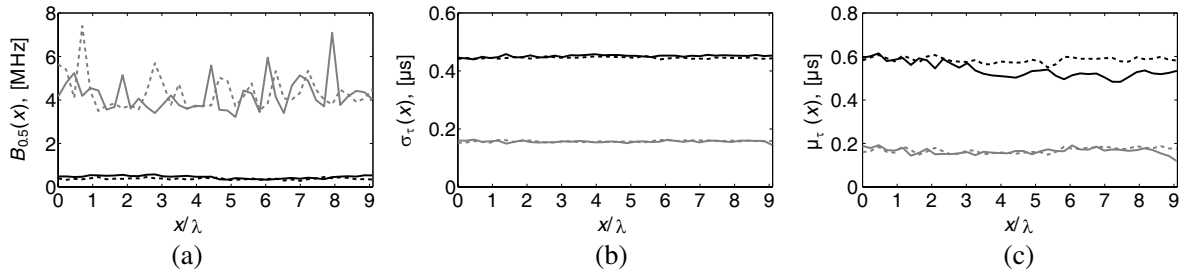

Figure 7. Expected value of (a) coherence bandwidth, (b) r.m.s. delay spread and (c) mean delay as a function of position along the virtual linear array. See Fig. 3(a) for legend and (10)–(12) for parameter definition.

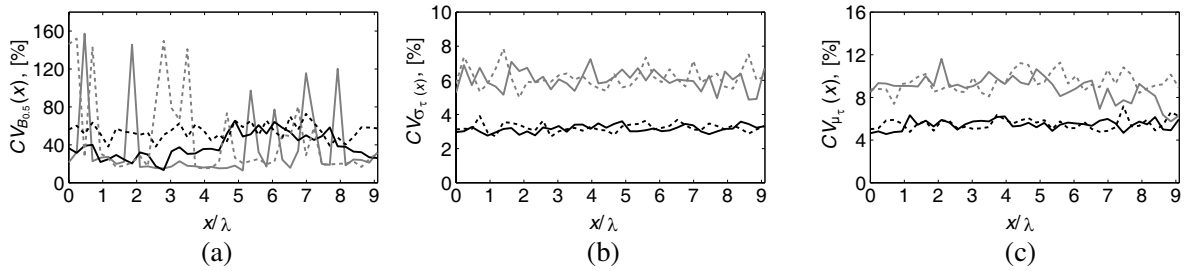

Figure 8. Coefficient of variation of (a) coherence bandwidth, (b) r.m.s. delay spread and (c) mean delay as a function of position along the virtual linear array. See Fig. 3(a) for legend and (13)–(15) for parameter definition.

coherence bandwidth as opposed to the case of no absorbers that emulates the same coherence along the array. Exactly the opposite behavior is observed for the r.m.s. delay spread as shown in Fig. 7(b), in this case, the use of absorbers decrease the r.m.s. delay spread by a factor approximately equal 2.5. This can be understood from the fact that for an ideal reverberation chamber with a perfect exponentially decaying power delay profile $B_{0.5}\sigma_\tau = \sqrt{3}/\pi$. However, in the general case, the product is governed by an uncertainty relationship. The average coherence bandwidth is rather homogeneous for all the considered scenarios. The mean delay is shown in Fig. 7(c). In the ideal case explained above, the mean delay and r.m.s. delay spread would have been equal.

Figures 8(a), (b) and (c) show the coherence bandwidth variability, the r.m.s. delay spread variability and the mean delay variability, respectively, all in percent ([%]) as a function of position along the virtual array. As we can see from the figures, the largest variability of all the considered variables is observed for the scenarios with absorbers as compared to the scenarios without absorbers. On one hand, it is just a few percents larger for the r.m.s. delay spread variability and the mean delay variability, while on the other it can be as much as 100% larger for the coherence bandwidth variability. This is an interesting result since we can conclude that despite the fact that the r.m.s. delay spread doesn't vary much along the virtual positions in the considered scenarios, the coherence bandwidth, on the other hand, could be varied to emulated different MIMO OFDMA channels.

Figure 9 shows the average correlation coefficient (defined in Section 2) for the four considered scenarios. The correlation coefficient ρ_{ij} is a matrix that depends on the positions i and j indicating the position of the (virtual) antennas in the array. The horizontal lines in Fig. 9 show the correlation level. For example, the continuous thick dark lines correspond to antenna $i = 7$, so the correlation coefficient is ρ_{7j} that reach its peak for $i = j = 7$ and decreases on both sides as we go further away. Hence, as expected, the correlation decreases as the separation distance between the antennas increases. As can be seen, the correlation for Direct measurements is higher than for Indirect measurements. This is expected since in Direct measurements the likelihood of observing a strong LOS component (i.e., higher K-factors) is larger than in Indirect measurements (see Fig. 5). An interesting observation is that the correlation is slightly higher for Direct measurements with absorbers than without absorbers. This behavior is in good agreement with the slightly higher K-factors obtained from Direct measurements with absorbers

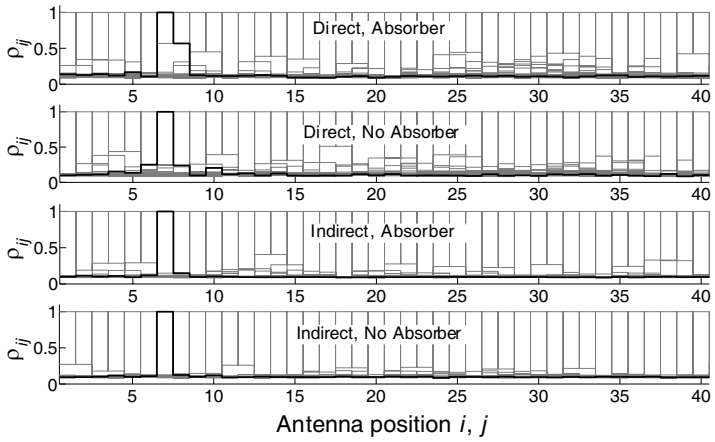

Figure 9. Frequency averaged antenna cross-correlation coefficient.

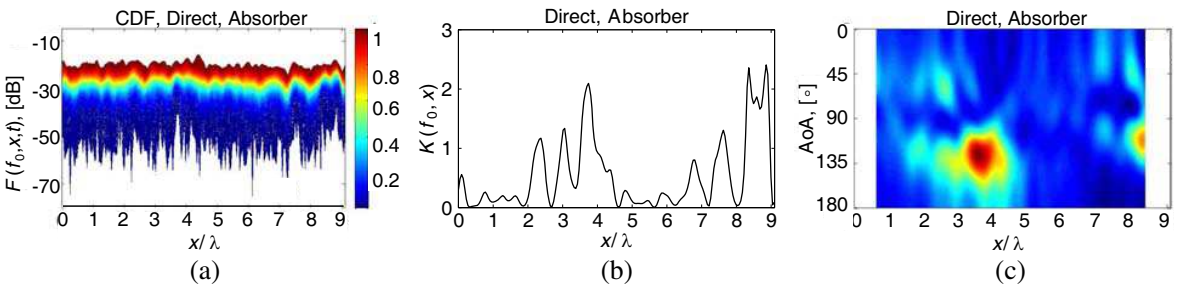

Figure 10. (a) CDF of instantaneous position-dependent power (the colorbar shows the probability level), (b) instantaneous position-dependent K-factor and (c) position-dependent beamforming AoA spectrum (normalized) as a function of the position along the virtual linear array. The considered frequency is $f_0 = 1\,\text{GHz}$. The color bar in (a) applies to (c) too.

as compared to similar measurements without absorbers as shown in Fig. 5(a). These results are consistent with each other; a further understanding requires an AoA analysis which is presented further on in Figs. 10 to 13. We can also see, that even if the introduction of absorbers has an impact on correlation, it is the pointing direction of the LPA antenna than plays the more fundamental role as in the case of the K-factor. However, the opposite is observed for the delay spread/coherence bandwidth, on which the absorbers have the major impact. These are essential factors that need to be taken into account in designing the propagation environment for testing VLM antenna designs and algorithms.

Above we presented a characterization of the propagation channel from a "global" perspective. We have seen that even if the global averages may seem rather constant (especially as a function of frequency), the variability of these parameters along the position of the very large virtual array may be changed by the user combining radio frequency absorbers with directive antennas. If we now change focus to the "local" perspective, we can see that the channel parameters really are different for the four considered scenarios. We are aware however of the fact that even if the changes are significant more variability could be achieved by finding some optimal arrangements of absorbers in conjunction with directive antennas. This, however, is outside the scope of the present work and might be addressed elsewhere in the future.

Figures 10(a), (b) and (c) show the Cumulative Distribution Function (CDF) of the instantaneous power $P(f_0, x, t)$, the corresponding K-factor $K(f_0, t)$, and the beamforming AoA spectrum as a function of the bowtie antenna along the virtual ULA for the "Direct, Absorber" scenario at the central frequency $f_0 = 1$. Figs. 11, 12 and 13 (with subfigures) show similar results for the "Direct, No Absorber" scenario, the "Indirect, Absorber" scenario and the "Indirect, No Absorber" scenario, respectively. As we can see, the "Direct, Absorber" scenario shows the largest variation of both power as well as K-factor, while the

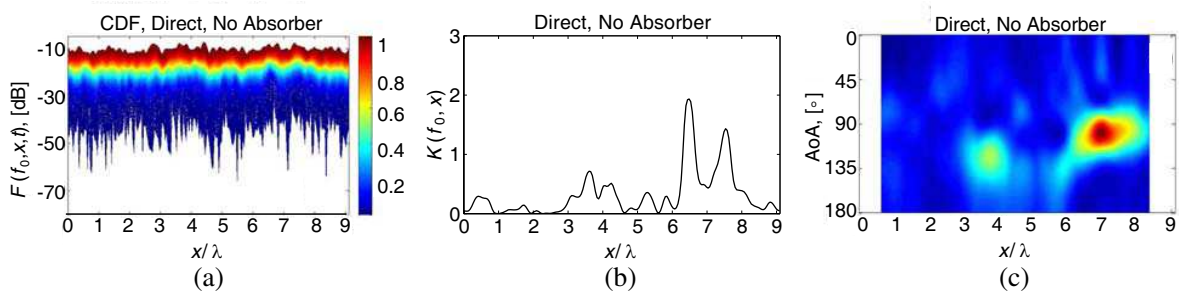

Figure 11. (a) CDF of instantaneous position-dependent power (the colorbar shows the probability level), (b) instantaneous position-dependent K-factor and (c) position-dependent beamforming AoA spectrum (normalized) as a function of the position along the virtual linear array. The considered frequency is $f_0 = 1\,\text{GHz}$. The color bar in (a) applies to (c) too.

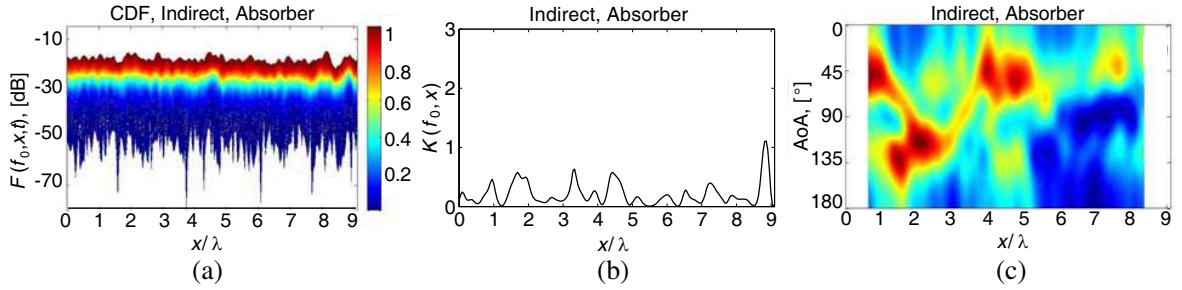

Figure 12. (a) CDF of instantaneous position-dependent power (the colorbar shows the probability level), (b) instantaneous position-dependent K-factor and (c) position-dependent beamforming AoA spectrum (normalized) as a function of the position along the virtual linear array. The considered frequency is $f_0 = 1\,\text{GHz}$. The color bar in (a) applies to (c) too.

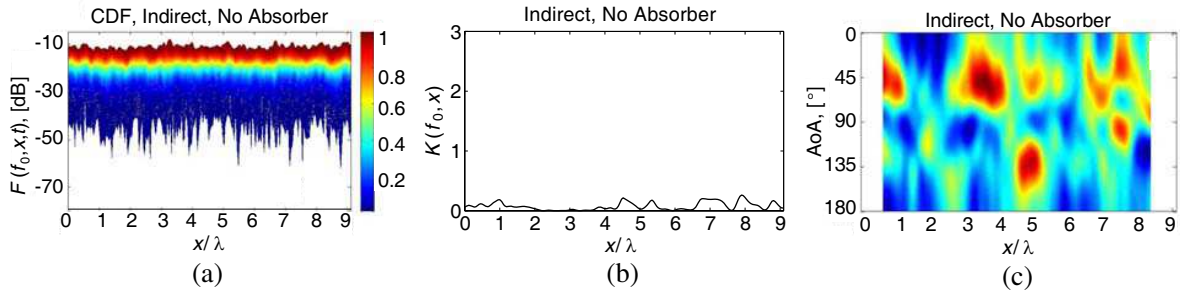

Figure 13. (a) CDF of instantaneous position-dependent power (the colorbar shows the probability level), (b) instantaneous position-dependent K-factor and (c) position-dependent beamforming AoA spectrum (normalized) as a function of the position along the virtual linear array. The considered frequency is $f_0 = 1\,\text{GHz}$. The color bar in (a) applies to (c) too.

"Indirect, No Absorber" shows the least variation (compare Figs. 10(a) and 10(b) with Figs. 13(a) and 7(b), respectively). The "Indirect, No Absorber" scenario is indeed a rich scattering isotropic scenario, as corroborated by the AoA spectrum shown in Fig. 13(c). A similar spectrum, however, slightly less isotropic is observed for the "Indirect, Absorber" scenario in Fig. 12(c). Clearly, the "Direct, No Absorber" scenario gives a spatially selective channel but less than the "Direct, Absorber" scenario. Comparing Fig. 10(c) and Fig. 11(c) explains the fact that the absorbers here have two functions: 1) they prevent part of the radiated signal to arrive at the receiver, especially in the direction of maximum gain of the LPA in the LOS direction and 2) splits part of the signal by diffraction on the edge of the stapled absorbers. These observations are consistent with our previous analysis of global statistics.

5. SUMMARY AND CONCLUSIONS

In this paper, we presented an experimental characterization of the radio propagation channel along a very large virtual array in a relatively large reverberation chamber mainly for use in Over The Air testing of MIMO antenna systems of various sizes, potentially including very large MIMO systems too. We have shown that the combined use of radio frequency absorbers and directive antennas can be used to produce different statistical environments in reverberation chambers. Hence, in addition to the well-known rich isotropic radio propagation channel intrinsically related to reverberation chambers operation, also other channels can be emulated with varying characteristics along the array, i.e, with non-isotropic angle of arrival distributions, varying coherence bandwidth and Rician fading statistics at different positions within the reverberation chamber. We found that absorbers, in addition to the well-known effect of increasing the rate of the power decay of the impulse response, also produce a change of the spatial statistics of the field magnitude distribution, i.e., fading statistics. Moreover, the frequency selectivity is also increased significantly at different positions in the chamber. However, a full understanding and control of the environment according to the user's needs requires further experimental and theoretical work. A fundamental goal would be to be able to tune, e.g., coherence bandwidth and r.m.s. delay spread, Ricean fading statistics antenna correlation, etc. given the system requirements. Future work should address a more specific way to incorporate the presented analysis to more standardized antenna testing methods.

ACKNOWLEDGMENT

Parts of the research leading to these results have received funding from the European Research Council under the European Community's Seventh Framework Programme (FP7/2007-2013)/ERC grant agreement No. 228044. The authors would like to thank Dr. Peter Fuks for his expert help during the measurement campaign.

REFERENCES

1. 3GPP, TR 25.814, "Physical layer aspects for evolved universal terrestrial radio access (Release 7)," 2006.
2. Marzetta, T. L., "Non-cooperative cellular wireless with unlimited numbers of base station antennas," *IEEE Trans. on Wireless Communications*, Vol. 9, No. 11, 3590–3600, Nov. 2010.
3. Rusek, F., D. Persson, B. K. Lau, E. G. Larsson, T. L. Marzetta, O. Edfors, and F. Tufvesson, "Scaling up MIMO: Opportunities and challenges with very large arrays," *IEEE Signal Processing Magazine*, Vol. 30, No. 1, 40–60, Jan. 2013.
4. Liu, X. and M. E. Bialkowski, "Effect of antenna mutual coupling on MIMO channel estimation and capacity," *International Journal of Antennas and Propagation*, Vol. 2010, Article ID 306173, 9 pages, 2010, doi:10.1155/2010/306173.
5. Payami, S. and F. Tufvesson, "Channel measurements and analysis for very large array systems at 2.6 GHz," *Proc. 6th European Conf. on Antennas and Propagation, EuCAP 2012*, Prague, Czech Republic, Mar. 2012.
6. Gao, X., F. Tufvesson, O. Edfors, and F. Rusek, "Measured propagation characteristics for very-large MIMO at 2.6 GHz," *Proc. 46th Annual Asilomar Conference on Signals, Systems and Computers*, Nov. 2012.
7. Glazunov, A. A., V. M. Kolmonen, and T. A. Laitinen, "MIMO over-the-air testing," *LTE-advanced and Next Generation Wireless Networks — Channel Modelling and Propagation*, Chapter 15, John Wiley & Sons, Oct. 2012.
8. 3GPP TS 34.114 V11.1.0, "User equipment (UE)/mobile station (MS) over the air (OTA) antenna performance," *Conformance Testing (Release 11)*, Jun. 2012.
9. Kildal, P.-S., X. Chen, C. Orlenius, M. Franzen, and C. S. L. Patane, "Characterization of reverberation chambers for OTA measurements of wireless devices: Physical formulations of channel

matrix and new uncertainty formula," *IEEE Trans. Antennas Propagat.*, Vol. 60, No. 8, 3875–3891, Aug. 2012.

10. Holloway, C. L., H. A. Shah, R. J. Pirkl, K. A. Remley, D. A. Hill, and J. Ladbury, "Early time behavior in reverberation chambers and its effect on the relationships between coherence bandwidth, chamber decay time, RMS delay spread, and the chamber buildup time," *IEEE Transactions on Electromagnetic Compatibility*, Vol. 54, No. 4, 714–725, Aug. 2012.
11. Valenzuela-Valdes, J. F., A. M. Martinez-Gonzalez, and D. A. Sanchez-Hernandez, "Emulation of MIMO nonisotropic fading environments with reverberation chambers," *IEEE Antennas and Wireless Propagation Letters*, Vol. 7, 325–328, 2008.
12. Sanchez-Heredia, J. D., J. F. Valenzuela-Valdes, A. M. Martinez-Gonzalez, and D. A. Sanchez-Hernandez, "Emulation of MIMO Rician-fading environments with mode-stirred reverberation chambers," *IEEE Transactions on Antennas and Propagation*, Vol. 59, No. 2, 654–660, Feb. 2011.
13. Rosengren, K. and P.-S. Kildal, "Study of distributions of modes and plane waves in reverberation chambers for characterization of antennas in multipath environment," *Microwave Opt. Technol. Lett.*, Vol. 30, No. 20, 386–391, Sep. 2001.
14. Holloway, C. L., D. A. Hill, J. M. Ladbury, P. Wilson, G. Koepke, and J. Coder, "On the use of reverberation chambers to simulate a controllable Rician radio environment for the testing of wireless devices," *IEEE Transactions on Antennas and Propagation*, Vol. 54, No. 11, 3167–3177, Nov. 2006.
15. Lienard, M. and P. Degauque, "Simulation of dual array multipath channels using mode-stirred reverberation chambers," *Electronics Letters*, Vol. 40, No. 10, 578–580, May 2004.
16. Kostas, J. G. and B. Boverie, "Statistical model for a mode-stirred chamber," *IEEE Trans. Electromagn. Compat.*, Vol. 33, 366–370, Nov. 1991.
17. Molisch, A. F., *Wireless Communications*, 2nd Edition, John Wiley & Sons, New York, 2011.
18. Garcia-Fernandez, M. A., J. D. Sanchez-Heredia, A. M. Martinez-Gonzalez, D. A. Sanchez-Hernandez, and J. F. Valenzuela-Valdes, "Advances in mode-stirred reverberation chambers for wireless communication performance evaluation," *IEEE Communications Magazine*, Vol. 49, No. 7, 140–147, Jul. 2011.
19. Kildal, P.-S. and K. Rosengren, "Correlation and capacity of MIMO systems and mutual coupling, radiation efficiency, and diversity gain of their antennas: Simulations and measurements in a reverberation chamber," *IEEE Communications Magazine*, Vol. 42, No. 12, 104–112, Dec. 2004.
20. Händel, P., S. Prasad, and C. Beckman, "Maximum likelihood estimation of reverberation chamber direct-to-scattered ratio," *Electronics Letters*, Vol. 45, No. 25, Dec. 2009.
21. Stoica, P. and R. Moses, *Introduction to Spectral Analysis*, Prentice-Hall, Englewood Cliffs, USA, 1997.